Laboratory study on heterogeneous decomposition of methyl chloroform on various standard aluminosilica clay minerals as a potential tropospheric sink

S. Kutsuna, Lin Chen, O. Ohno, N. Negishi, K. Takeuchi, T. Ibusuki, K. Tokuhashi, A. Sekiya

Atmos. Chem. Phys. Discuss., 3, 1843–1891, 2003
www.atmos-chem-phys.org/acpd/3/1843/

Atmospheric Chemistry and Physics Discussions

Laboratory study on heterogeneous decomposition of methyl chloroform on various standard aluminosilica clay minerals as a potential tropospheric sink

S. Kutsuna, L. Chen, K. Ohno, N. Negishi, K. Takeuchi, T. Ibusuki, K. Tokuhashi, and A. Sekiya

National Institute of Advanced Industrial Science and Technology (AIST), 16-1 Onogawa, Tsukuba, Ibaraki 305-8569, Japan

Received: 31 January 2003 – Accepted: 20 March 2003 – Published: 1 April 2003

Correspondence to: S. Kutsuna (s-kutsuna@aist.go.jp)

Abstract

Methyl chloroform (1,1,1-trichloroethane, CH_3CCl_3) was found to decompose heterogeneously on seven types of standard clay minerals (23 materials) in dry air at 313 K in the laboratory. All reactions proceeded through the elimination of HCl; CH_3CCl_3 was converted quantitatively to $CH_2{=}CCl_2$. The activities of the clay minerals were compared via their pseudo-first-order reaction rate constants (k_1). A positive correlation was observed between the k_1 value and the specific surface area (S) of clay minerals, where the S value was determined by means of the general Brunauer-Emmett-Teller (BET) equation. The k_1 value was anti-correlated with the value of n, a parameter of the general BET equation, and correlated with the water content that can be removed easily from the clay minerals. The reaction required no special pretreatment of clay minerals, such as heating at high temperatures; hence, the reaction can be expected to occur in the environment. Photoillumination by wavelengths present in the troposphere did not accelerate the decomposition of CH_3CCl_3, but it induced heterogeneous photodecomposition of $CH_2{=}CCl_2$. The temperature dependence of k_1, the adsorption constants of CH_3CCl_3 and $CH_2{=}CCl_2$, and a surface reaction rate constant were determined for an illite sample. The k_1 value increased with increasing temperature. The amount of CH_3CCl_3 adsorbed on the illite during the reaction was proportional to the partial pressure of CH_3CCl_3. The reaction was sensitive to relative humidity and the k_1 value decreased with increasing relative humidity. However, the reaction was found to proceed at a relative humidity of 22% at 313 K, although the k_1 value was about one-twentieth of the value in dry air. The conditions required for the reaction may be present in major desert regions of the world. A simple estimation indicates that the possible heterogeneous decomposition of CH_3CCl_3 on the ground surface in arid regions is worth taking into consideration when inferring the tropospheric lifetime of CH_3CCl_3 and global OH concentration from the global budget concentration of CH_3CCl_3.

ACPD

3, 1843–1891, 2003

1. Introduction

The atmospheric lifetime of methyl chloroform (1,1,1-trichloroethane, CH_3CCl_3) is required to evaluate influence of CH_3CCl_3 on the environment, for example, stratospheric ozone layer depletion and global warming (IPCC, 2001). The lifetime has been inferred from long-term ground-based observatory data on the atmospheric concentration of CH_3CCl_3 in the ALE/GAGE/AGAGE (three sequential experiments: the Atmospheric Lifetime Experiment, the Global Atmospheric Gases Experiment, and the Advanced Global Atmospheric Gases Experiment) (Prinn et al., 1983a; WMO, 1998) or in NOAA/CMDL (National Oceanic and Atmospheric Administration/Climate Monitoring and Diagnostics Laboratory) databases (WMO, 1998), by model calculations (Prinn et al., 1995; Krol et al., 1998; Prinn et al., 2001) using the CH_3CCl_3 emissions data estimated (McCulloch and Midgley, 2001). In this procedure, a gas-phase reaction with OH is considered a main atmospheric sink of CH_3CCl_3, and photolysis and dissolution into seawater (Butler et al., 1991; Tie et al., 1992) are regarded as minor atmospheric sinks of CH_3CCl_3. The atmospheric chemistry of CH_3CCl_3 is thus related to global and hemispheric OH concentration. The atmospheric lifetime of CH_3CCl_3 through a reaction with OH inferred is scaled and used for estimating the lifetimes of chemical substances such as hydrochlorofluorocarbons and hydrofluorocarbons (Prather and Spivakovsky, 1990; Spivakovsky et al., 2000). The tropospheric lifetime of CH_3CCl_3 through a reaction with OH is evaluated at 6.0 years (Prinn et al., 2001).

The atmospheric concentration of CH_3CCl_3 increased in the 1980s. However, it has been decreasing dramatically since 1992 because of regulation under the Montreal Protocol. This decrease in atmospheric CH_3CCl_3 provides an opportunity to study the behavior of OH in the atmosphere (Ravishankara and Albritton, 1995; Spivakovsky et al., 2000; Montzka et al., 2000; Prinn et al., 2001). Recently, an interhemispheric difference of OH concentration and a decline in OH concentration in the last two decade have been suggested on the basis of data on the atmospheric concentration of CH_3CCl_3 (Montzka et al., 2000; Prinn et al., 2001). On the other hand, these behaviors

ACPD
3, 1843–1891, 2003

are not supported by a 3-D model calculation or by observations of ^{14}CO (Krol et al., 1998; Manning et al., 2002). It has also been pointed out that the current estimate of global OH budget is more sensitive to errors in the CH_3CCl_3 emissions data because of a lower atmospheric concentration of CH_3CCl_3 (Jöckel et al., 2002). A significant underestimation of the emission rate of CH_3CCl_3 in Europe in 2000 and 2001 has been reported (Krol and Lelieveld, 2002). The use of chemical tracers other than CH_3CCl_3 to estimate the global OH budget has been discussed (Jöckel et al., 2002; Huang and Prinn, 2002).

In this laboratory study, we investigated an additional tropospheric sink of CH_3CCl_3, that is, heterogeneous decomposition of CH_3CCl_3 on clay minerals. If it served as a significant sink, the global OH concentration deduced would be influenced. It is known that CH_3CCl_3 can easily decompose heterogeneously on sands and metal surfaces under dry conditions (Rebbert and Ausloos, 1979). Some of us reported that dehydrochlorination of CH_3CCl_3 occurred easily on clay minerals (allophane and halloysite) at 313 K and indicated the possibility that the heterogeneous decomposition of CH_3CCl_3 on clay minerals at the ground surface in arid regions would serve as a potential tropospheric sink (Kutsuna et al., 2000a). Clay minerals are among the main components of soils and dusts. The importance of heterogeneous reactions on dust and soil has been reported by model, field, and laboratory studies on ozone, SO_2, NO_2, and so on (Dentener et al.,1996; Güsten et al., 1996; Underwood et al., 2001; Hanisch and Crowley, 2002; Ooki and Uematsu, 2002).

This paper has three main parts. In the first part, we examine the reaction of CH_3CCl_3 on nine types of standard clay minerals (25 American Petroleum Institute (API) standard clay minerals, Kerr and Kulp, 1949) with a closed-circulation reactor. We found that the decomposition of CH_3CCl_3 proceeded through $CH_3CCl_3 \rightarrow CH_2{=}CCl_2 + HCl$ at 313 K for most of the clay minerals examined. The relationship of the reaction rate to the surface area and mineralogy of the clay minerals is discussed. In the second part, the adsorption coefficient and the surface reaction rate constant of CH_3CCl_3 on illite and their temperature dependence are determined. Illite is a dominant clay

ACPD
3, 1843–1891, 2003

mineral in arid regions (Claquin et al., 1999). Illite is observed in dusts from desert regions (Khalaf et al., 1985; Singer, 1988; Blanco et al., 2002; Bruintjes et al., 2002). The reaction rate increased with increasing temperature and it decreased with increasing relative humidity. Finally, on the basis of the adsorption coefficient and the surface reaction rate obtained for the illite, the atmospheric lifetime of CH_3CCl_3 through decomposition on clay minerals is discussed. A simple estimation indicates that dry deposition due to heterogeneous decomposition on clay minerals in arid regions may serve as a tropospheric sink of CH_3CCl_3.

2. Experimental

2.1. Clay samples and measurement of their specific surface area

The 25 kinds of standard clay materials referring to those from the American Petroleum Institute (API) (Kerr and Kulp, 1949) that were examined are listed in Table 1. Illite (API no. 35) and illite (API no. 35*) are different lots for the same kind of clay mineral. Four kinds of clay minerals examined in the previous study (Kutsuna et al., 2000a) are also listed for comparison in Table 1. All of the samples were purchased from Iwamoto Mineral Co., Japan. Some clay materials were grained, and all of the particles were less than 1 mm in diameter.

In order to determine the specific surface area of the clay samples, we measured the adsorption and desorption isotherms of N_2 on the clay samples at 77 K using a gas sorption system (Quantachrome AUTOSORB 1). The isotherms were measured at relative pressures ranging from 10^{-3} to slightly under 1.0 by the static volumetric method. As described later (Sect. 3.1), the general (i.e. three-parameter) form of the Brunauer-Emmett-Teller (BET) equation was used to determine the specific surface area of the clay samples.

The clay samples examined belong to two types of aluminosilicate layer minerals. The kaolinite, halloysite, and dickite clays are 1:1 aluminosilicate layer minerals; that

ACPD
3, 1843–1891, 2003

is, these clay minerals consist of one layer of silica (Si^{4+}) in tetrahedral coordination and one layer of aluminum (Al^{3+}) in octahedral coordination with oxygen and hydroxyl in the anion positions. The montmorillonite, metabentonite, nontronite, hectorite, and pyrophyllite clays are 2:1 aluminosilicate layer minerals; that is, these clay minerals consist of two layers of Si^{4+} in tetrahedral coordination and one layer of Al^{3+} in octahedral coordination with oxygen and hydroxyl in the anion positions. The latter layer is sandwiched by the former layers. Pyrophyllite consists of these aluminosilica layers without any exchange ions in place of Al^{3+} or Si^{4+}. In montmorillonite, a magnesium ion (Mg^{2+}) is typically substituted for Al^{3+} in octahedral coordination. Substitution of Al^{3+} for Si^{4+} in tetrahedral coordination may also occur. In nontronite, ferric ion (Fe^{3+}) is substituted for Al^{3+} in octahedral coordination, while Al^{3+} is substituted for Si^{4+} in tetrahedral coordination. In hectorite, Mg^{2+} and a lithium ion (Li^{+}) substitute for Al^{3+} in octahedral coordination. The above substitutions result in a negative charge on the three-layer sheet, which in turn is balanced by intersheet adsorbed cations such as calcium (Ca^{2+}) and sodium (Na^{+}) ions. The intersheet Ca^{2+} and/or Na^{+} interact with water molecules. It is known that the negatively charged clay surface, the exchangeable cations, aluminum at crystal edges, and transition metals in the higher valency state are related to the reactivity of clay minerals (Solomon, 1968; Mortland and Raman, 1968; Swoboda and Kunze, 1968; Theng, 1974). The formulas of the API clay materials were reported by Kerr et al. (1950).

2.2. Experimental runs with the closed-circulation reactor

The experiments were performed in a 0.85-dm^3 closed-circulation Pyrex reactor, which is described elsewhere in more detail (Kutsuna et al., 2000a), so only a brief summary will be given here. The reactor consists of a removable cell in which clay samples are put, a magnetic-driven glass pump, and a White-type optical cell with an optical path length of 3 m by which the gas mixture is analyzed using an FTIR spectrometer (JEOL Winspec 50) at a 0.5 cm^{-1} resolution with 50 scans.

ACPD
3, 1843–1891, 2003

The clay samples were pretreated before each experimental run. A 50-mg sample of clay mineral particles was piled loosely on a small plate in the removable cell and exposed at atmospheric pressure to synthetic air at a rate of 0.2 dm^3 min^{-1} at a fixed temperature (typically 393 K) for an hour. The samples were subsequently cooled to the desired reaction temperature, which was typically 313 K. In the experiments carried out in a humidified atmosphere, the clay samples were exposed to a 0.2 dm^3 min^{-1} flow of humidified synthetic air of a known relative humidity for an additional 3.5 h at the reaction temperature.

The gas mixture of CH_3CCl_3 in air was prepared by mixing a standard gas mixture of CH_3CCl_3 in nitrogen molecules (N_2) (Takachiho-Kogyo Co., Japan) with N_2 or oxygen molecules (O_2). The initial partial pressure of CH_3CCl_3 was typically set at 16 Pa. In some experiments, the relative humidity was established by passing a part of the gas mixture through water (Ichinose-type humidifier).

The experimental procedure was as follows: the reactant gas mixture was circulated for 30 min without contact with the clay sample, and then the gas circulation path was changed so that the gas mixture flowed over the clay sample for 180 min without exposure to photoillumination. In most of the experiments, the gas mixture and the clay sample were then photoilluminated for 80 min at wavelengths longer than 300 nm with a 500-W xenon short-arc lamp (Ushio Co. Ltd., Japan), a mirror, and an optical filter (HOYA UV 30). The light intensity was about 6 mW cm^{-2} at 365 nm as measured with a UV sensor (USHIO UVD-365PD). The reaction temperature was controlled between 283 and 313 K (±0.5 K) by putting the removable cell in a constant-temperature water bath.

2.3. Experimental runs with the column reactor

A column reactor system is in principle a kind of gas chromatograph. 85 mg of clay particles was held by small plugs of quartz wool in a Teflon tube (column reactor) with an inside diameter of 2.4 mm. This column was put in a temperature-controlled water bath to keep the reaction temperature at 313 K. Helium (He) was used as a carrier gas,

and it was passed through the clay sample at a rate of 5×10^{-3} dm^3 min^{-1}. The pressure before the column reactor was automatically controlled at atmospheric pressure by a valve (248A, MKS Co., Japan) that was located after the column reactor. The pressures before and after the column reactor were measured at 100.5 and 99.9 kPa. No pretreatment such as heating at a higher temperature was performed. In the experiment in a humidified atmosphere, the He carrier was passed through water (Ichinose-type humidifier). The relative humidity was controlled by changing the temperature of the water. A prescribed volume (5×10^{-3} dm^3) of a He mixture containing xenon (Xe) by 1×10^{-4} volume ratio or CH_3CCl_3 by 5×10^{-4} volume ratio was injected using a multi-port valve. The shape of the peak, that is, the retention time (delay time after the injection) and the peak height, of Xe or CH_3CCl_3 was measured with a quadrapole mass-spectrometer. The He flow was added to the line after the column reactor to decrease the residence time in the line (dead time).

3. Results and discussion

3.1. Surface area of the clay samples

Figure 1 shows the adsorption/desorption isotherms of nitrogen molecules for four API clay mineral standards at 77 K. Isotherms are generally classified by their shape (Sing et al., 1985). The kaolinite isotherm (API no. 7) was Type II, and the other isotherms were Type IV. For all the minerals except for kaolinite (API no. 7), we observed hysteresis between the adsorption and the desorption isotherms. The types of these hysteresis loops were classified as Types H3, H2, and H4 for halloysite (API no. 12), montmorillonite (API no. 20), and illite (API no. 35), respectively. The hysteresis indicates that mesopores contribute to the surface area, whereas closure of the hysteresis at $P/P_0 \approx 0.4$ suggests that there was not a significant volume of slits accessible to N_2 below this width (≈ 2.2 nm) and that finer voids were wedge shaped. A similar hysteresis was observed for nontronite and hectorite samples, as well as for other samples

ACPD
3, 1843–1891, 2003

of halloysite, montmorillonite and illite. For kaolinite and dickite samples, there was little hysteresis between the adsorption and desorption isotherms. For the pyrophyllite sample, a Type H4 hysteresis was observed down to $P/P_0 = 0.1$.

The surface area was initially calculated for the adsorption isotherm, in the relative pressure range $P/P_0 = 0.05 - 0.30$, using the popular (i.e. two-parameter) BET equation (Eq. 1). The BET method is the most widely used procedure for the determination of the surface area of solid materials and involves the use of the following BET equation (Eq. 1) (Sing et al., 1985).

$$W = \frac{W_m C(P/P_0)}{[1 - (P/P_0)][1 + (C - 1)(P/P_0)]}, \quad (1)$$

where W is the weight of gas adsorbed at a given relative pressure (P/P_0); W_m is the weight of adsorbate constituting a monolayer of surface coverage; and P_0 is the saturated vapor pressure at the temperature of the adsorbent. The term C, which is the BET C constant, is related to the energy of adsorption in the first adsorbed layer and consequently its value is an indication of the magnitude of the adsorbent/adsorbate interactions. The C value should be positive. The BET specific surface area and values of the BET parameter C obtained are listed in Table 1. Although the C value should be positive, the calculation using Eq. (1) resulted in negative C values for most of the clay samples.

Then, the surface area was calculated by the general (i.e. three-parameter) form of the BET equation (Eq. 2) (Murray and Quirk, 1990).

$$W = \frac{W_m(P/P_0)[1 - (n+1)(P/P_0)^n + n(P/P_0)^{n+1}]}{[1 - (P/P_0)][1 + (C-1)(P/P_0) - C(P/P_0)^{n+1}]}, \quad (2)$$

where n is the number of adsorbate layers to which multilayer formation is limited. When $n = 1$, Eq. (2) is the Langmuir equation and, for large values of n, it assumes the form of Eq. (1). In practice, therefore, Eqs. (1) and (2) are virtually coincident for values of n larger than ~5 and $P/P_0 < 0.3$. Equation (2) was applied to the adsorption

ACPD
3, 1843–1891, 2003

isotherms in the relative pressure range P/P_0 = 0.05 – 0.30, by a nonlinear fitting method. The specific surface area and the parameters C and n obtained are listed in Table 1. This surface area will be referred to as the g-BET specific surface area S in the text. In this calculation, when $n > 5$, n was fixed at a value of 10. Eq. (2) gave positive C values for all clay samples. This result agrees with that reported by Murray and Quirk (1990). Hence, the g-BET surface area S and the relating parameters n and C are used in the following discussion.

3.2. Heterogeneous decomposition on various standard clay minerals

3.2.1. HCl elimination reaction

Figure 2 depicts the infrared spectra of a CH_3CCl_3-air mixture before contact with a halloysite sample (API no. 12) at 313 K and at 4 and 64 min after contact. As the intensity of the CH_3CCl_3 peaks decreased with time, new peaks appeared at 788, 869, and 1627 cm^{-1}. These new peaks are attributed to 1,1-dichloroethene (CH_2=CCl_2). No decomposition products other than CH_2=CCl_2 were detected in the air mixture.

Figure 3, part A, shows the time course of the partial pressure of CH_3CCl_3 (P_{MC}) and that of CH_2=CCl_2 (P_{DE}) in this reaction. At 30 min, a CH_3CCl_3-air mixture began to flow over the halloysite material. The rapid decrease at that time was caused by gas adsorption on the halloysite and by changes in the circulation route that led to changes in the reactor volume. The volume change was calculated to correspond to a 23% decrease in partial pressure. After contact with the clay sample, CH_3CCl_3 decreased approximately according to first-order kinetics.

Figure 3, part B, plots the increase in P_{DE}, which is described as ΔP_{DE} hereafter, against the decrease in P_{MC}, which is described as $-\Delta P_{MC}$ hereafter, during a 180-min reaction period. Except for the initial reaction period, the increase in ΔP_{DE} was almost the same as the increase in $-\Delta P_{MC}$. Hence, the reaction was judged to proceed

ACPD
3, 1843–1891, 2003

through elimination of HCl (Mochida et al., 1968; Vogel et al., 1987) as follows:

$$CH_3CCl_3 \rightarrow CH_2=CCl_2 + HCl. \quad (3)$$

Photoillumination was not required in this reaction. Hydrogen chloride (HCl) produced could be bound to the surface of the clay samples.

At 210 min, photoillumination ($\lambda > 300$ nm) was started against CH_3CCl_3 – CH_2=CCl_2 – air mixtures in the presence of the clay material. As shown in Fig. 3, part A, photoillumination did not accelerate decomposition of CH_3CCl_3, but it induced heterogeneous photodecomposition of the CH_2=CCl_2 that had been produced. HCl and carbon dioxide (CO_2) were detected as photodecomposition products of CH_2=CCl_2. Under photoillumination, the partial pressure of CH_3CCl_3 seems to be almost constant. This effect was also observed for the reactions on other clay minerals. It will be discussed later (Sect. 3.2.3). In the text, the reactions under photoillumination are described only in Sect. 3.2.3; otherwise, "reaction" means the reaction without photoillumination.

In a similar way, decomposition of CH_3CCl_3 and formation of CH_2=CCl_2 were confirmed in dry air at 313 K for most of the API standard clay minerals examined. Since CH_3CCl_3 decreased exponentially with time, the decay rate was evaluated by using the quasi-first-order rate constant k_1. That is, the k_1 value for each experiment was calculated by fitting the data at time t (ranging from 14 to 114 min) after contact with a clay sample to the equation $P(t) = P_0 \exp(-k_1 t)$, where $P(t)$ and P_0 are the partial pressures of the CH_3CCl_3 at time t and at time 0 after beginning of contact, respectively. The k_1 values obtained are shown in Table 1. The values in parentheses represent the errors deduced by the non-linear regression. The errors in this text indicate $\pm\sigma$. The removal ratio K at 0 min of reaction time is defined as $K = (P_{0calc} - P_0)/P_0$, where $P_{0calc} = 0.77\times$ (the average partial pressure before contact with the clay mineral). N in Table 1 indicates the number of experimental runs. When several experiments were carried out ($N > 1$), the mean and the standard deviation of the mean are listed in Table 1. Except for the dickite (API no. 15) and the pyrophyllite (API no. 49) samples,

ACPD
3, 1843–1891, 2003

the decomposition of CH_3CCl_3 on clay minerals in dry air at 313 K was confirmed by the positive value of k_1.

Figure 4 plots ΔP_{DE} against $-\Delta P_{MC}$ for 114 min of reaction time for all clay samples examined. The two values are almost the same for each mineral, which implies that the decomposition on the clay minerals examined occurred through the HCl elimination reaction shown in Eq. (3). HCl was not observed in the gas phase except for the reaction on the hectorite sample (API no. 34). Thus, HCl seems to be bound to the surface of most of the clay minerals. The result for the hectorite sample (API no. 34) will be discussed later (in Sect. 3.2.4).

3.2.2. Relation of k_1 with the surface area and mineralogy of the clay minerals

The order of the k_1 values for the different minerals typed was as follows: hectorite, nontronite > halloysite, metabentonite > kaolinite ≫ dickite, pyrophyllite. For the montmorillonite samples, the k_1 value varied from 10^{-5} to 41×10^{-5} s^{-1} for 50 mg of sample. In a previous study (Kutsuna, 2000a), the montmorillonite sample examined showed a small value of k_1 (montmorillonite-p in Table 1), but in this study several of the montmorillonite samples exhibited much larger k_1 values. As for the illite samples examined, the k_1 value of one material (no. 35 or 35*) was ten times that of the other material (no. 36).

Figure 5, part A, plots the k_1 value against the g-BET specific surface area (S) for each clay sample. The k_1 value correlated positively with the S value. The positive correlation between the k_1 and S values is in contrast to the relation observed in the heterogeneous decomposition of some hydrofluoroethers on similar clay materials (Kutsuna et al., 2002; however, in that study, the surface area was calculated by Eq. 1). The slope k_1/s is estimated to be 5.6×10^{-5} s^{-1} m^{-2} with a correlation coefficient (R) of 0.72, where s is the surface area of 50 mg of the clay material, that is, $s = 0.05 \times S$. Considering the reactor volume (0.85 dm^3), k_1/n_s (m s^{-1}) is calculated to be 4.8×10^{-8}, where n_s is the surface area concentration of the clay mineral [m^2 (m^3 of air)$^{-1}$]. The

k_1/n_s value corresponds to the uptake coefficient γ of 9×10^{-10} when 223 m s^{-1} was given for mean molecular velocity of CH_3CCl_3. Figure 5, part B, shows the K value versus the g-BET surface area. The adsorption was almost proportional to the g-BET surface area. The slope K/s is estimated to be 6.6×10^{-2} m^{-2} ($R = 0.85$). Considering the distribution factor of CH_3CCl_3 between in air and on the clay material, the reaction rate on clay minerals k_{clay} is approximately expressed by $k_{clay} = k_1(1 + K)/K$. The power k_1 $(1 + K)$ was plotted against the g-BET surface area in Fig. 8, part C. Both the values showed a positive correlation. The $k_1(1 + K)/s$ slope was 6.8×10^{-5} s^{-1} m^{-2} ($R = 0.79$).

The k_1/s values are listed in Table 1. Although the k_1 value is roughly proportional to the s value, the k_1/s values vary by two orders of magnitude. For example, the hectorite sample (API no. 34) has the largest value of k_1/s. Among the 12 montmorillonite materials, the k_1/s values vary from 0.8×10^{-5} to 7.8×10^{-5} s^{-1} m^{-2}. For one illite sample (API no. 35 or 35*), k_1/s was about five times larger than for the other illite sample (API no. 36).

In general, not all of the internal surface area of porous solids always participates in the reaction (Keyser et al., 1991). The clay materials examined have mesopores and micropores, as mentioned in Sect. 3.1. Therefore, it is necessary to check whether the BET surface area corresponds to all of the surface area accessible to CH_3CCl_3. The ratio of the surface area participating in the reaction is indicated by the effectiveness factor η. As for an irreversible first-order reaction with a reaction rate constant of k_{1e} (s^{-1}), the η value of flat materials with narrow cylindrical pores and of porous spherical materials can be calculated by Eq. (4) or (4'), respectively, as follows (Levenspiel, 1999):

$$\eta = \frac{\tanh\phi}{\phi} \quad \text{for flat materials with narrow cylindrical pores} \tag{4}$$

$$\eta = \frac{3}{\phi}\left(\frac{1}{\tanh\phi} - \frac{1}{\phi}\right) \quad \text{for porous spherical materials,} \tag{4'}$$

ACPD
3, 1843–1891, 2003

where ϕ is Tiele's modulus, which is calculated by Eqs. (5) or (5'):

$$\phi = L(k_{1e}/D_{MC})^{1/2} \quad \text{for flat materials with narrow cylindrical pores} \tag{5}$$

$$\phi = R(k_{1e}/D_{MC})^{1/2} \quad \text{for porous spherical materials,} \tag{5'}$$

where L is length of cylindrical pores; D_{MC} is the effective diffusion coefficient of CH_3CCl_3 in the pores; and R is the radius of the pores. In both types of porous materials, the η value becomes almost unity when $\phi < 1$. In the reactions examined, L and R can be less than 10^{-3} m. The order of the k_{1e} value can be estimated from the k_1 values as $< 10^{-3}\,s^{-1}$. The D_{MC} value depends on the structure of the pores and is difficult to estimate, but it should not be $< 10^{-9}\,m^2\,s^{-1}$. Hence, η can be evaluated as < 1, and the ϕ value is expected to be about unity. Thus, the variability of k_1/s is not due to the different η values of the clay materials.

Figure 6, part A, plots the k_1/s value against the g-BET parameter n. The k_1/s values tend to be large for clay materials with small n. For example, the hectorite sample (API no. 34), which exhibits the largest k_1/s value, has the smallest n value. There is a distinct difference in n between the two illite materials (API nos. 35 or 35* and 36). The reason for this relation between k_1/s and n is not clear. A possible explanation is as follows. As described in Sect. 3.1, a small value of n means that there are many narrow voids accessible to N_2 (for example, cumulative voids about 0.4~1.4 nm in diameter for $n = 2$). These voids are formed by connections between clay crystals via their faces and/or edges. The anti-correlation of n and k_1/s suggests that such narrow voids may serve as reaction sites. These voids may accelerate the reaction under special circumstances such as in intense electric fields (Aochi and Farmer, 1995).

For the montmorillonite samples, the relation between k_1/s and n is ambiguous. For example, materials with similar small values of k_1/s (API nos. 25, 26, and 27) have values of n from 3.3 to 10. The correlation of the k_1/s value with the mineralogy of the montmorillonite materials was checked on the basis of their reported chemical

analyses (Kerr et al., 1950). The chemical formulas of the clay samples (API nos. 22A and 30A) were assumed to be, respectively, the same as the clay samples (API nos. 22 and 30). No correlation of the k_1/s value with the charge at the clay surface nor with the substituted metal in tetrahedral and octahedral coordination was found. The k_1/s value seemed to correlate with the concentration of interlayer Ca^{2+} and with the water content of the clay minerals examined. Figure 6, parts B and C, plots the k_1/s value against the concentration of the interlayer Ca^{2+} and the water content, respectively. The water content shown in Fig. 6, part C, presents the amount of the water that the clay could release at < 378 K. The Ca-montmorillonite materials tended to exhibit larger k_1/s values than the Na-montmorillonite materials with the exception of one montmorillonite (API no. 24). The positive correlation between the k_1/s value and the amount of water loosely bound to the clay indicates that sites formed by removal of water can serve as active sites for the decomposition of CH_3CCl_3. It is known that solid acid sites can serve as active sites for the decomposition of CH_3CCl_3 (Mochida et al., 1968). Solid acid sites seem to be present under dry conditions (Zielke et al., 1989). The adsorption/desorption behavior of water seems to be a key to the reactivity of clay minerals against the decomposition of CH_3CCl_3, as mentioned later in Sects. 3.2.3 and 3.3.2.

3.2.3. Effects of pretreatment, reaction temperature, and photoillumination

In this study, the clay samples were dried at 393 K for 1 h in air flow before the reaction. This commonly used procedure for drying clay minerals is said to not destroy their structure. On the other hand, it is well known that the activity of clay minerals, for example, their acidity, depends on the water content of the surface (Zielke et al., 1989). Hence, the effect of the pretreatment temperature was examined for three clay materials (API nos. 20, 34, and 35*). Figure 7 plots the k_1 values measured for the reaction on each clay material against the pretreatment temperature. The k_1 values seem to decrease with decreasing pretreatment temperature. However, the difference was less than the measurement error for k_1. The decomposition of CH_3CCl_3 was confirmed at

pretreatment temperatures down to 323 K. The purpose of the pretreatment is the removal of some of the water from the clay minerals. In general, clay minerals lose water at temperatures a little higher than ambient temperature. Reaction conditions similar to the pretreatment in this study can be found in natural environments, particularly in hot and dry regions such as the Sahara Desert.

The k_1 value increased with increasing reaction temperature. Figure 8, parts A and B, shows a semi-logarithm plot of the typical time course of P_{MC} in typical reactions on hectorite (API no. 34) and illite (API no. 35*), respectively, at 283–313 K. The decay rate for each reaction at each different temperature was evaluated by the quasi-first-order rate constant k_1, as described in Sect. 3.2.1. Some data determined during the initial reaction period did not obey first-order kinetics, probably because the adsorption equilibrium was not yet established. Accordingly, the data was fitted for the reaction times between 14 and 114 min for the reaction at 313 K, and for those between 74 and 174 min for the reactions at 298 and 283 K. Figure 8, part C, plots the k_1 values obtained against the inverse of the reaction temperature. For the reaction at 313 K on hectorite (API no. 34) and the reactions at 283–313 K on illite (API no. 35*), several experiments were run. Figure 8, part C, plots the mean of the k_1 values for those reactions at each temperature. The error bars show the standard deviation of the mean at each temperature for illite (API no. 35*), while the error bars for hectorite (API no. 34) were set at the ratio of error to the mean at 313 K (46%). The apparent activation energies (ΔE) of the reactions on hectorite (API no. 34) and illite (API no. 35*) were calculated as (71 ± 24) and (37 ± 21) kJ mol^{-1}, respectively, by the weighted-nonlinear regression of the data using the Arrhenius equation, $k_1 = A_r \exp[(-\Delta E/R)/T]$. These apparent activation energies are smaller by about 150 and 180 kJ mol^{-1}, respectively, than that for the homogeneous gas-phase thermal decomposition of CH_3CCl_3 (220 kJ mol^{-1}) (Weissman and Benson, 1984). In contrast, they are larger than the activation energy (12.9 kJ mol^{-1}) (DeMore et al., 1997) for the gaseous reaction with OH, which is a main tropospheric process for the removal of CH_3CCl_3. The relative importance of the reaction on clay minerals to the gaseous reaction with OH thus increases with

ACPD
3, 1843–1891, 2003

increasing temperature.

CH_3CCl_3 did not decompose by photoillumination ($\lambda > 300$ nm), as shown in Fig. 3, part A, for any clay materials. In contrast, $CH_2{=}CCl_2$, which had been produced, decomposed through a heterogeneous photoreaction on the clay minerals except for some montmollironite (API nos. 25 and 27). For the dickite (API no. 15) and the pyrophyllite (API no. 49), photodecomposition of $CH_2{=}CCl_2$ was not examined in this study, because $CH_2{=}CCl_2$ had not been produced from CH_3CCl_3 on these clay minerals. The photodecomposition of $CH_2{=}CCl_2$ on the API standard clay minerals is similar to the photoreaction observed for halloysite-p and kaolinite-p in the previous study (Kutsuna et al., 2000b). CO_2 were detected as a gaseous photodecomposition product of $CH_2{=}CCl_2$. When the photodecomposition rate was large, HCl was observed.

As described in Sect. 3.2.1 (Fig. 3, part A), the decay rate of CH_3CCl_3 was decreased under photoillumination, and this was the case for most of clay minerals. This behavior can be ascribed in part to gradually decreasing activity of clay minerals during a 180-min reaction before photoillumination. But, compared with effect of this inactivation, the decrease in decay rate of CH_3CCl_3 was large in most of the reactions. For a case of the reaction on halloysite (API no. 12) as shown in Fig. 3, when photoillumination was started, CH_3CCl_3 increased due to desorption from the clay surface. The desorption decreased the decay rate of CH_3CCl_3 under photoillumination. CH_3CCl_3 seems to be released by increasing temperature of the clay surface under photoillumination. The desorption can also be explained by accumulation of photodecompositon products such as HCl on the clay surface. This explanation is supported by the fact that CH_3CCl_3 decreased under photoillumination after disappearance of $CH_2{=}CCl_2$ (Fig. 3). The inhibiting effect of the photodecomposition products of $CH_2{=}CCl_2$ can be expected to be less significant in the environment because diffusion of newly formed $CH_2{=}CCl_2$ to the atmosphere decreases $CH_2{=}CCl_2$ over clay minerals to much lower concentrations in the environment than in this study.

ACPD
3, 1843–1891, 2003

3.2.4. Reaction on hectorite

The hectorite material (API no. 34) had the largest k_1/s value. In the reaction on hectorite, HCl was observed as a gaseous product. The ready release of HCl from the clay surface is probably the reason that the k_1/s value is so large. After HCl increased in the air mixture, it decreased by being adsorbed onto the hectorite. As shown in Fig. 8, the apparent activation energy for the reaction on hectorite (API no. 34) was larger than that for the reaction on illite (API no. 35*). The large value of k_1/s for hectorite (API no. 34) does not result from the lower activation energy of the reaction on hectorite. Hectorite (API no. 34) has some remarkable features in comparison with the other clay minerals examined: the presence of Li and F atoms, the trioctahedral sheet, and the presence of micropores. These features may be related to the ready release of HCl into the air and the large number of reaction sites, which may result in the large k_1/s value.

3.3. Reaction on illite

3.3.1. Temperature dependence of the adsorption and surface reaction

The temperature dependence of the adsorption was considered separately from that of the surface reaction of CH_3CCl_3 for the reactions on illite (API no. 35*). Figure 9 plots ΔP_{DE} against $-\Delta P_{MC}$ for each reaction on illite (API no. 35*) shown in Fig. 8, part A. The discrepancy between ΔP_{DE} and $-\Delta P_{MC}$ increased as the temperature decreased from 313 to 283 K. The discrepancy observed during the initial reaction period and that for the reactions at lower temperatures can be explained by the presence of CH_3CCl_3 or $CH_2{=}CCl_2$ or both, which did not react, adsorbed onto the clay surface. This explanation is supported by the fact that the formation rate of $CH_2{=}CCl_2$ and the rate of decrease of CH_3CCl_3 were almost the same after the initial reaction periods.

In order to evaluate the amount of $CH_2{=}CCl_2$ adsorbed (a_{DE} in molecules) in these reactions, the adsorption of $CH_2{=}CCl_2$ was measured at temperatures of 283–313 K

ACPD
3, 1843–1891, 2003

using the closed-circulation reactor. The results are shown in Fig. 10. The data were analyzed by using the Langmuir adsorption Eq. (6):

$$a_{DE} = \frac{mSq^{DE}K_p^{DE}P_{DE}}{1 + K_p^{DE}P_{DE}}, \quad (6)$$

where m is the mass of the clay mineral in g; S is the specific surface area of the clay minerals in $m^2\ g^{-1}$; q^{DE} is a temperature-independent parameter in m^{-2}; and K_p^{DE} is an equilibrium constant in Pa^{-1}. The parameters q^{DE} and K_p^{DE} are obtained by a nonlinear regression of all the data at different temperatures with the same value of q^{DE}. The regression gave $q^{DE} = 2.0 \times 10^{17}$ (m^{-2}) and K_p^{DE} = 1.5, 3.2, 6.0, 9.0, and 15.1 (10^{-3} Pa) at 313, 306, 298, 291, and 283 K, respectively. The a_{DE} values calculated from these values are shown by solid curves in Fig. 10, part A. The product $q^{DE}\ K_p^{DE}$ is plotted against the inverse of temperature in Fig. 10, part B. The K_p^{DE} value obeys the equation $K_p^{DE}(T_2) = K_p^{DE}(T_1)\exp[(\Delta E_{ads}/R)(T_1^{-1} - T_2^{-1})]$, where $K_p^{DE}(T_1)$ and $K_p^{DE}(T_2)$ are the adsorption constants at temperatures T_1 and T_2, respectively; ΔE_{ads} is the heat of adsorption (J mol^{-1}); and R is the universal gas constant (J mol^{-1} K^{-1}). The value of ΔE_{ads} was calculated as $-(56 \pm 10)$ kJ mol^{-1} by the weighted-nonlinear regression.

The amount of CH_3CCl_3 adsorbed onto the clay surface (a_{MC} in molecules) was calculated as follows:

$$a_{MC} = 2.07 \times 10^{17}(-\Delta P_{MC} - \Delta P_{DE}) - a_{DE}, \quad (7)$$

where the factor 2.07×10^{17} in molecules Pa^{-1} is a result of the units used in Eq. (7). In all reactions, a_{MC} was much larger than a_{DE}. Figure 11 plots a_{MC} versus P_{MC} for all experimental runs at 313 K (part A), 298 K (part B), and 283 K (part C). Except for the data from the initial reaction period, colored in gray, each data set can be fitted by a straight line intersecting the origin. A Henry's law type equation (Eq. 8) thus applied

ACPD
3, 1843–1891, 2003

under the reaction conditions examined.

$$a_{MC} = m\,S\,K_H^{MC}\,P_{MC}, \quad (8)$$

where m is the mass of the clay mineral in g; S is the specific surface area of the clay mineral in $m^2\ g^{-1}$; and K_H^{MC} is an equilibrium constant in $m^{-2}\ Pa^{-1}$. The K_H^{MC} values derived by regressing the data in Fig. 10 are listed in Table 2 along with the k_1 value obtained as described before.

In order to consider the temperature-dependence of adsorption and surface reaction separately, we simplified the reaction scheme as follows:

$$CH_3CCl_3(g) \longleftrightarrow CH_3CCl_3(pore) \quad (9)$$

$$CH_3CCl_3(pore) \longleftrightarrow CH_3CCl_3(ad) \quad (10)$$

$$CH_3CCl_3(ad) \longrightarrow CH_2 = CCl_2(ad) + HCl(ad) \qquad k_{sr} \quad (11)$$

$$CH_2 = CCl_2(ad) \longleftrightarrow CH_2 = CCl_2(g). \quad (12)$$

In this scheme, under quasi-equilibrium conditions, the value of k_1 is represented by k_{sr} (s^{-1}) and K_H^{MC} ($m^{-2}\ Pa^{-1}$) as follows:

$$k_1 = 1.71 \times 10^{-17} k_{sr} K_H^{MC} / (1 + 1.71 \times 10^{-17} K_H^{MC}), \quad (13)$$

where the factor 1.71×10^{-17} in m^2 Pa is a result of the units used in Eq. (13). The k_{sr} value can be calculated by using Eq. (13) with the measured k_1 and K_H^{MC} values. The K_H^{MC} and k_{sr} values are listed in Table 2. The K_H^{MC} are also plotted in Fig. 10, part B. The stronger adsorption of CH_3CCl_3 compared with that of $CH_2{=}CCl_2$ is indicated by $K_H^{MC} > q^{DE} K_P^{DE}$. The heat of adsorption of CH_3CCl_3 is calculated to be $-(38 \pm 6)$ kJ mol^{-1} by weighted-nonlinearly regressing the data by using the equation $K_H^{MC}(T_2) = K_H^{MC}(T_1) \exp[(\Delta E_{ads}/R)(T_1^{-1} - T_2^{-1})]$. The k_{sr} values are plotted in Fig. 8, part C. By weighted-nonlinearly regressing the data in Fig. 8, part C, by using the Arrhenius equation, the $k_{sr}(T)$ value in s^{-1} was expressed by Eq. (14).

$$k_{sr}(T) = 4.78 \times 10^9 \exp(-8930/T). \quad (14)$$

ACPD
3, 1843–1891, 2003

The activation energy of the surface reaction ΔE_r obtained is (74 ± 31) kJ mol^{-1}.

3.3.2. Effects of relative humidity

The dry surface of clay minerals seems to play an important role in the decomposition of CH_3CCl_3, as mentioned in Sect. 3.2.3. We also found previously that the decomposition rate of CH_3CCl_3 on clay minerals (halloysite and allophane) decreased with increasing relative humidity (Kutsuna et al., 2000a). Figure 12 shows the k_1 value and the amount of CH_2=CCl_2 produced in a 114-min reaction at different relative humidities. Both the k_1 value and the amount of CH_2=CCl_2 decreased with increasing relative humidity. At 43% relative humidity, the formation of CH_2=CCl_2 was not detected and the k_1 value was about one-fiftieth of the value in dry air. At 22% relative humidity, CH_2=CCl_2 formation and the k_1 value were about 18 and 20 times smaller, respectively, than in dry air. The decomposition of CH_3CCl_3 proceeded even at 22% relative humidity, however, at 313 K.

The effect of relative humidity was examined by means of a column reactor experiment. Figure 13, part A, shows the xenon peak (Xe) after a Xe-He mixture and a dry He carrier-gas flow were passed through the column, which contained 85 mg of illite material (API No. 35*), at 313 K. Figure 13, parts B–D, shows the CH_3CCl_3 peaks after a CH_3CCl_3-He mixture and He carrier-gas flow with controlled relative humidity were passed through the column at 313 K. Xe was used as a reference because little is adsorbed onto clay minerals. The corrected retention time rt(MC) is defined as t(MC)–t(Xe), where t(Xe) and t(MC) are the respective retention times of the Xe and CH_3CCl_3 peaks. The value of rt(MC) is approximately proportional to the adsorption constant of CH_3CCl_3 on the illite sample (API no. 35*). The adsorption of CH_3CCl_3 on the clay minerals at 43% and 17% relative humidity decreased by about 34 and 16 times, respectively, compared with adsorption in a dry atmosphere. The column experiment indicates that water content on the surface decreases the adsorption of CH_3CCl_3 on the clay surface. In addition, it confirms that CH_3CCl_3 can be adsorbed on the clay

ACPD
3, 1843–1891, 2003

surface at 17% relative humidity.

3.4. Environmental implications of the reaction of CH_3CCl_3 on clay minerals

3.4.1. Estimated lifetime through decomposition on clays in airborne dusts

The values obtained for k_{sr} and K_H^{MC} in Sect. 3.3.1 indicate that mass-transport processes such as a gas diffusion process cannot be the rate-limiting step for removal by airborne dust. In this case, the removal rate of CH_3CCl_3 ($\tau_{dust}^{local-1}$ in year^{-1}) is determined as follows. First, the distribution factor of CH_3CCl_3, f_{MC}, is defined as the ratio of its mass concentration on clay minerals c_{ad} [g (m^3 of air)$^{-1}$] to its gas-phase mass concentration c_g [g (m^3 of air)$^{-1}$]:

$$f_{MC} = c_{ad}/c_g. \quad (15)$$

By using Eqs. (8) and (15), we arrive at,

$$f_{MC} = K_A^{MC} R\,T\,S\,n_m, \qquad K_A^{MC} = 1.17 \times 10^{-22} K_H^{MC}, \quad (16)$$

where n_m is the mass concentration of the clay minerals [g (m^3 of air)$^{-1}$]; R is the universal gas constant equal to 8.31 Pa m^3 mol^{-1} K^{-1}; and the factor 1.17×10^{-22} in mol is a result of the units in Eq. (16). The K_A^{MC} value in m^{-2} Pa^{-1} mol is expressed by Eq. (17).

$$K_A^{MC} = 4.53 \times 10^{-13} \exp(4570/T). \quad (17)$$

The proportion of CH_3CCl_3 on clay minerals, X_{ad}^{MC}, is given by

$$X_{ad}^{MC} = f_{MC}/(1 + f_{MC}). \quad (18)$$

Combining Eqs. (16) and (18) yields

$$X_{ad}^{MC} = K_A^{MC} RT\,S\,n_m/(1 + K_A^{MC} R\,T\,S\,n_m). \quad (19)$$

ACPD
3, 1843–1891, 2003

Assuming that the reaction rate is proportional to a_{MC} with a surface reaction rate constant of k_{sr} (s^{-1}) as described in the Sect. 3.3.1, $\tau_{dust}^{local-1}$ can be determined by Eq. (20):

$$\tau_{dust}^{local-1} = 3.15 \times 10^7 k_{sr} K_A^{MC} R\,T\,S\,n_m/(1 + K_A^{MC} R\,T\,S\,n_m), \quad (20)$$

where the factor 3.15×10^7 (y^{-1} s) is a result of the units in Eq. (20).

From Eqs. (14), (17), and (20), the local lifetime of CH_3CCl_3 through the reaction on clay particles (τ_{dust}^{local}) can be calculated for different concentrations of clay minerals (n_m) in the atmosphere. The result is shown in Table 3. Blanks in Table 3 indicate > 1000 years of lifetime.

Tegen and Fung (1994) modeled the atmospheric mineral dust cycle using a global three-dimensional model that included source regions and different size fractions of the soil components and their size distributions. The results indicated that the annual average concentration of clay-sized dust exceeds several $\mu g\ m^{-3}$ in the first dynamic layer (about 960 mbar) over and around the continents almost everywhere. Even if all of those clay-sized dust exhibit a similar activity for the decomposition of CH_3CCl_3 as illite (API no. 35*), τ_{dust}^{local} would be estimated to be > 1000 years. This is much longer than the tropospheric lifetime of CH_3CCl_3 through the reaction with OH (6.0 years) (Prinn et al., 2001). We hence conclude that the reaction on airborne clays cannot serve as a significant tropospheric sink of CH_3CCl_3.

At the local scale, the reactions on airborne clay dusts will be significant only for high (e.g. hundreds of $\mu g\ m^{-3}$) concentrations of airborne clay minerals. The relative humidity dependence of the reaction shown in Sect. 3.3.2 indicates that the conditions required for the reaction may be present in arid and semi-arid regions. Here we consider the reaction on airborne dust over such dry regions. Model calculations indicate that the seasonal dust concentration in the planetary boundary layer (0 to 1 km altitude) exceeds $250\,\mu g\ m^{-3}$ over the western Sahara and the Sahel region, in parts of the Arabic Peninsula and Iran, and in the Asian source regions (Taklimakan and Gobi deserts) (Ginoux et al., 2001). The model calculation also shows that the volume frac-

ACPD
3, 1843–1891, 2003

tion of clay-sized particles (< 2 μm of diameter in the coarse mode) in those dusts are approximately a half. Illite is estimated to be a dominant clay mineral in the Sahara Desert (Claquin et al., 1999). By sampling of airborne dusts and observation of their composition in the laboratory, illite minerals in dusts from deserts are detected with an IR spectrum (Blanco et al., 2002) or an XPS spectrum (Bruintjes et al., 2002). If half of the dust has an activity similar to that of illite (API no. 35*), the τ_{dust}^{local} value would be estimated to be a few hundred years at 283 K and about 60 years or less at 313 K. The decomposition on airborne clays may hence contribute locally to the removal of CH_3CCl_3 in dust storms and plums, although it cannot be significant at the global scale.

3.4.2. Estimated lifetime through decomposition on clays at the ground surface

Higher concentrations of clay minerals are expected for reactions occurring close to the surface. In arid regions, the type of reaction studied here is expected to be significant because it proceeds easily under dry conditions. Temperatures in excess of 333 K at the surface of the Sahara Desert during the daytime should accelerate the reactions. Illite has been reported to be a dominant clay mineral in desert regions (Claquin et al., 1999), although the absolute concentrations are not known. Kaolinite, montmorillonite, and other clays have also been reported in desert regions (Potter and Rossman, 1977; Péwé et al., 1981; Verrecchia and Le Coustumer, 1996). The tropospheric lifetime of CH_3CCl_3 by the reaction at ground level (τ_{ground}^{tropos}) was estimated from the model reported by Alyea et al. (1978). We assumed a fairly dry desert surface. In this model, τ_{ground}^{tropos} is estimated as follows:

$$\tau_{ground}^{tropos} = 12.04/(a\,N_d)(\text{years}), \quad (21)$$

where N_d is the area expressed as a multiple of the area of the model desert (1500 km wide and 3000 km long) and a is the chemical removal efficiency of CH_3CCl_3 at the ground surface, which was determined experimentally as shown below (Alyea et al.,

1978). The global desert areas are roughly equal to five model deserts (N_d = 5). The a value is taken to be the removal ratio of CH_3CCl_3 to the initial concentration experimentally determined for reaction periods of 3.5 days in a reactor 1 m high in which particles have been spread over the bottom. The parameter a takes on values between 0 and 1. The a value was calculated by Eqs. (14), (17) and (20) by assuming concentration of clay minerals (C_w in the ratio of the weight of clays to that of all the sands at top layer of the ground surface) having an activity similar to that of illite (API no. 35*), reaction temperature T, and parameter of d_L. The τ^{tropos}_{ground} value was estimated from the a value thus obtained and Eq. (21) for different values of N_d. The result was listed in Table 4. Blanks in Table 4 indicate > 1000 years of lifetime.

In Table 4, the case of N_d = 5 means that lifetime is evaluated for all desert regions in the world. The area of N_d = 2 is almost equal to that of the Sahara Desert. The parameter d_L means the top layer depth of the ground surface in which clays can contact with CH_3CCl_3 in the atmosphere. The d_L value is not known. The case of d_L = 2 μm means that only clays exposed to the atmosphere can contact with CH_3CCl_3. The lengths of d_L = 20 μm and 2 mm correspond to maximum diameters defined for silt-sized and small sand-sized particles, respectively. A soil density of 2.5 g cm^{-3} was used in the calculation. The calculation was performed for three cases (i)–(iii). In case (i), the value of C_w corresponds to a half of a clay-sized sand fraction (< 2 μm in diameter of sands) reported from the field observations of the dry deposition of ozone onto the Lybian Desert in the Sahara Desert (Güsten et al., 1996). In case (iii), one-twentieth (0.05 K^{MC}_A) of the value calculated by Eq. (17) was substituted for K^{MC}_A in Eq. (20). The other parameters were set to be the same as those in the case (i). The case (iii) may correspond to the reaction under humidified conditions, for example, at about 20% relative humidity at 313 K.

In estimation of the dry deposition rate for O_3 to the desert sand, an aerodynamic resistance and a quasi-laminar boundary-layer resistance were reported to be insignificant compared with the bulk surface resistance (Güsten et al., 1996). The extent of deposition rates examined here for CH_3CCl_3 was < 10^{-6} cm s^{-1}, which corresponded

ACPD
3, 1843–1891, 2003

to several years of τ_{ground}^{tropos} or longer lifetime. This deposition rate was less than that reported for O_3; hence, in calculating *a*, an aerodynamic resistance and a quasi-laminar boundary-layer resistance were not considered, and only bulk surface resistance was estimated.

Table 4 indicates that dry deposition originating from decomposition on clay minerals can be a significant removal process at ground level, involving $> 10^{-4}$ by weight (100 ppmw) of clay minerals such as illite (API no. 35*) (Table 4). Hence, we conclude that the reactions in the top layer of the soil could serve as a significant tropospheric sink for CH_3CCl_3, if the relative humidity does not decrease the reaction rate significantly. The difference in the reaction activity among illite materials (Table 1) is a remaining research subject. On the other hand, the reaction in semiarid regions that have larger amounts of clays than arid regions do could be significant, as could the transport of clay particles to arid and semiarid regions. The decomposition of CH_3CCl_3 over deserts might be found on the basis of the ALE/GAGE/AGAGE or NOAA/CMDL data. For example, at the station in Barbados, which is located in the North Atlantic Ocean, for the ALE/GAGE/AGAGE network, dust plumes passing over the Sahara Desert have been observed (Mahowald et al., 2002). The long-term continuous data on the atmospheric concentration of CH_3CCl_3 at the station might provide an opportunity to evaluate locally the contribution of heterogeneous decomposition over the Sahara Desert to CH_3CCl_3 lifetime.

4. Conclusions

By using the closed-circulation reactor, the reactions of CH_3CCl_3 on various types of the standard clay minerals were examined typically at 313 K and in dry air. The following conclusions were obtained.

– CH_3CCl_3 decomposes to $CH_2{=}CCl_2$ quantitatively on seven types (23 samples) of clay minerals via the elimination of HCl at temperatures appropriate to the lower

ACPD
3, 1843–1891, 2003

troposphere. The decomposition occurs without photoillumination. Photoillumination does not accelerate the decomposition.

- The pseudo-first-order reaction rate constant is roughly proportional to the surface area of the clay sample. The surface area of clay sample such as porous montmorillonite should be estimated by the general (three-parameter) BET equation instead of the two-parameter BET equation.
- A parameter of the general BET equation n, the interlayer Ca^{2+} content, and the water content that can be removed easily from the clay minerals seem to be related to the activity of the clay materials.
- The decomposition of CH_3CCl_3 on clay minerals requires no special pretreatment of clay minerals, such as heating at high temperatures; hence, the reaction can be expected to occur in the environment.
- The reaction rate increases with increasing temperature and decreases with increasing relative humidity. This dependence indicates that the conditions required for the reaction may be present in hot and dry regions such as the Sahara Desert.
- The adsorption equilibrium constants and the surface reaction rate constants for an illite sample can be determined in the temperature range of 283–313 K.
- The decomposition on clays in airborne dusts can be expected not to be a significant tropospheric sink of CH_3CCl_3. It may be significant locally in dust events and dust plumes.
- The dry deposition due to the reaction on clays at the ground level in arid regions can be expected to serve as a tropospheric sink of CH_3CCl_3.
- Influence of a potential sink of CH_3CCl_3, decomposition on clays, on the inferred atmospheric OH concentration may be different between in the Northern

ACPD
3, 1843–1891, 2003

Hemisphere and in the Southern Hemisphere, since deserts are distributed more widely in the Northern Hemisphere.

– The inhibiting effect of relative humidity on the decomposition of CH_3CCl_3 on clay minerals is an important research subject that should be further evaluated in the laboratory.

References

Alyea, F. N., Cunnold, D. M., and Prinn, R. G.: Meteorological constraints on tropospheric halocarbon and nitrous oxide destructions by siliceous land surfaces, Atmos. Environ., 12, 1009–1011, 1978.

Aochi, Y. O. and Farmer, W. J.: Spectroscopic evidence for the rate-limited accumulation of a persistent fraction of 1,2-dichloroethane sorbed onto clay minerals, Environ. Sci. Technol., 29, 1760–1765, 1995.

Blanco, A., Castellano, A., Filippo, E., Manno, D., Perrone, M. R., and Serra, A.: Characterisation of African dust over south Italy, in Proceedings of 2002 Joint International Symposium on Atmospheric Chemistry within the Earth System, 49, Crete, 2002.

Bruintjies, R., Piketh, S. J., Mangoosh, A., Mandoos, A., Breed, D., Jensen, T., Salazar, V., and Ross, K. E.: Microphysical and radiative properties of clouds in the Middle East – United Arab Emirates, in Proceedings of 2002 Joint International Symposium on Atmospheric Chemistry within the Earth System, 91, Crete, 2002.

Butler, J. H., Elkins, J. W., Thompson, T. M., and Hall, B. D.: Oceanic consumption of CH_3CCl_3:Implications for tropospheric OH, J. Geophys. Res., 96, 22 347–22 355, 1991.

Claquin, T., Schulz, M., and Balkanski, Y. J.: Modeling the mineralogy of atmospheric dust sources, J. Geophys. Res., 104, 22 243–22 256, 1999.

Dentener, F., Carmichael, G. R., Zhang, Y., Lelieveld, J., and Crutzen, P. J.: Role of mineral aerosol as a reactive surface in the global troposphere, J. Geophys. Res., 101, 22 869–22 889, 1996.

DeMore, W. B., Sander, S. P., Golden, D. M., Hampson, R. F., Kurylo, M. J., Howard, C. J., Ravishankara, A. R., Kolb, C. E., abd Molina, M. J.: Chemical kinetics and photochemical data for use in stratospheric modeling, JPL Publ. 97-4, 1997.

Ginoux, P., Chin, M., Tegen, I., Prospero, J. M., Holben, B., Dubovik, O., and Lin S.-J.: Sources and distributions of dust aerosols simulated with the GOCART model, J. Geophys. Res., 106, 20 255–20 273, 2001.

Güsten, H., Heinrich, G., Mönnich, E., Sprung, D., Weppner, J., Ramadan, A. B., Ezz El-Din, M. R. M., Ahmed, D. M., and Hassan, G. K. Y.: On-line measurements of ozone surface fluxes: part II. Surface-level ozone fluxes onto the Sahara desert, Atmos. Environ., 30, 911–918, 1996.

Hanisch, F. and Crowley, J. N.: Ozone decomposition on Saharan dust: an experimental investigation, Atmos. Chem. Phys. Discuss., 2, 1809–1845, 2002.

Huang, J. and Prinn, R. G.: Critical evaluation of emissions for potential new OH titating gases, in Proceedings of 2002 Joint international Symposium on Atmospheric Chemistry within the Earth System, 22, Crete, 2002.

IPCC: Climate Change 2001: The Scientific Basis. Contribution of Working Group I to the Third Assessment Report of the Intergovernmental Panel on Climate Change (Houghton, J. T., Y. Ding, D. J. Griggs, M. Noguer, P. J. van der Linden, X. Dai, K. Maskell, and C. A. Johnson (eds.)), Cambridge University Press, Cambridge, UK and New York, 881, 2001.

Jöckel, P., Brenninkmeijer, C. A. M., and Crutzen, P. J.: A discussion on the determination of atmospheric OH and its trends, Atmos. Chem. Phys. Discuss., 2, 1261–1286, 2002.

Kerr, P. F. and Kurp, J. L.: Reference clay localities – united states, in American Petroleum Institute Project 49 Clay Minerals Standards, preliminary report No. 2, 1–106, Columbia University, New York, 1949.

Kerr, P. F., Hamilton, P. K., Pill, R. J., Wheeler, G. V., Lewis, D. R., Burkhardt, W., Reno, D., Taylor, G. L., La Habra Laboratory, Mielenz, R. C., King, M. E., and Schieltz, N. C.: Analytical data on reference clay materials, in American Petroleum Institute Project 49 Clay Minerals Standards, preliminary report No. 7, 38–58, Columbia University, New York, 1950.

Keyser, L. F., Moore, S. B., and Leu M.-T.: Surface reaction and pore diffusion in flow-tube reactors, J. Phys. Chem., 95, 5496–5502, 1991.

Khalaf, F. I., Al-Kadi, A., and Al-Saleh, S.: Mineralogical composition and potential sources of dust fallout deposits in Kuwait, northern arabian gulf, Sedimentary Geology, 42, 255–278, 1985.

Krol, M., van Leeuwen, P. J., and Lelieveld, J.: Global OH trend inferred from methylchloroform measurements, J. Geophys. Res., 103, 10 697–10 711, 1998.

Krol, M. and Lelieveld, J.: Substantial emissions of 1,1,1-trichloroethane over Europe in 2000

and 2001: Consequences for global OH inversions, in Proceedings of 2002 Joint International Symposium on Atmospheric Chemistry within the Earth System, 22–23, Crete, 2002.
Kutsuna, S., Takeuchi, K., and Ibusuki, T.: Laboratory study on heterogeneous degradation of methyl chloroform (CH_3CCl_3) on aluminosilica clay minerals as its potential tropospheric sink, J. Geophys. Res., 105, 6611–6620, 2000a.
Kutsuna, S., Ibusuki, T., and Takeuchi, K.: Heterogeneous photoreaction of tetrachloroethene-air mixture on halloysite particles, Environ. Sci. Technol., 34, 2484–2489, 2000b.
Kutsuna, S., Chen, L., Nohara, K., Takeuchi, K., and Ibusuki, T.: Heterogeneous decomposition of $CHF_2OCH_2CF_3$ and $CHF_2OCH_2C_2F_5$ over various standard aluminosilica clay minerals in air at 313 K, Environ. Sci. Technol., 36, 3118–3123, 2002.
Levenspiel, O.: Chemical reaction engineering, 3rd ed., 385–391, New York, John Wiley & Sons, 1999.
Mahowald, N. M., Zender, C. S., Luo, C., Savoie, D., Torres, O., and del Corral, J.: Understanding the 30-year Barbados desert dust record, J. Geophys. Res., 107, 4561, doi:10.1029/2002JD002097, 2002.
Manning, M. R., Lowe, D. C., Moss, R., and Brailsford, G.: Trends and anomalies in southern hemisphere OH inferred from 12 years of ^{14}CO data, in Proceedings of 2002 Joint International Symposium on Atmospheric Chemistry within the Earth System, 22-23, Crete, 2002.
McCulloch, A. and Midgley, P. M.: The history of methyl chloroform emissions: 1951–2000, Atmos. Environ., 35, 5311–5319, 2001.
Mochida, I., Take, J., Saito, Y., and Yoneda, Y.: Linear free-energy relationships in heterogeneous catalysis, VI, Catalytic elimination reaction of hydrogen chloride from chloroethanes on solid acids and bases, J. Org. Chem., 32, 3894–3898, 1968.
Montzka, S. A., Spivakovsky, C. M., Butler, J. H., Elkins, J. W., Lock, L. T., and Mondeel, D. J.: New observation constraints for atmospheric hydroxyl on global and hemispheric scales, Science, 288, 500–503, 2000.
Mortland, M. M. and Raman, K. V.: Surface acidity of smectites in relation to hydration, exchangeable cation, and structure, Clays and Clay Minerals, 16, 393–398, 1968.
Murray, R. S. and Quirk, J. P.: Intrinsic failure and cracking of clay, Soil Sci. Soc. Am. J., 54, 1179–1184, 1990.
Ooki, A. and Uematsu, M.: Chemical interactions on the surface of the mineral dust particles with the acid gases during the ACE-ASIA intensive experiment, in Proceedings of 2002 Joint International Symposium on Atmospheric Chemistry within the Earth System, 73, Crete,

2002.
Péwé, T. L., Péwé, E. A., Péwé, R. H., Journaux, A., and Slatt, R. M.: Desert dust: characteristics and rates of deposition in central Arizona, in Desert Dust: origin, characteristics, and effect on man, Special Paper 186, edited by T. L. Péwé, 169–190, Geol. Soc. of Am., Boulder, CO, 1981.
Potter, R. M. and Rossman, G. R.: Desert varnish: the importance of clay minerals, Science, 196, 1446–1448, 1977.
Prather, M. and Spivakovsky, C. M.: Tropospheric OH and the lifetimes of hydrochlorofluorocarbons, J. Geophys. Res., 95, 18 723–18 729, 1990.
Prinn, R. G., Rasmussen, R. A., Simmonds, P. G., Alyea, F. N., Cunnold, D. M., Lane, B. C., Cardelino, C. A., and Crawford, A. J.: The atmospheric lifetime experiment, 5, Results for CH_3CCl_3 based on 3 years of data, J. Geophys. Res., 88, 8415–8426, 1983.
Prinn, R. G., Weiss, R. F., Miller, B. R., Huang, J., Alyea, F. N., Cunnold, D. M., Frazer, P. J., Hartley, D. E., and Simmonds, P. G.: Atmospheric trends and lifetime of CH_3CCl_3 and global OH concentrations, Science, 269, 187–192, 1995.
Prinn, R. G., Huang, J., Weiss, R. F., Cunnold, D. M., Fraser, P. J., Simmonds, P. G., McCulloch, A., Harth, C., Salameh, P., O'Doherty, S., Wang, R. H. J., Porter, L., and Miller, B. R.: Evidence for substantial variations of atmospheric hydroxyl radicals in the past two decades, Science, 292, 1882–1888, 2001.
Ravishankara, A. R. and Albritton, D. L.: Methyl chloroform and the atmosphere, Science, 269, 183–184, 1995.
Rebbert, R. E. and Ausloos, P.: Stratospheric ozone depletion by halocarbons: Chemistry and transport, 68, Nat. Acad. of Sci., Washington, 1979.
Sing, K. S. W., Everett, D. H., Haul, R. A. W., Moscou, L., Pierotti, R. A., Rouquérol, J., and Siemieniewska, T.: Reporting physisorption data for gas/solid systems with special reference to the determination of surface area and porosity, Pure & Appl. Chem., 57, 603–619, 1985.
Singer, A.: Illite in aridic soils, desert dusts and desert loess, Sedimentary Geology, 59, 251–259, 1988.
Solomon, D. H.: Clay minerals as electron acceptors and/or electron donors in organic reactions, Clays and Clay Minerals, 16, 31–39, 1968.
Spivakovsky, C. M., Logan, J. A., Montzka, S. A., Balkanski, Y. J., Foreman-Fowler, M., Jones, D. B. A., Horowitz, L. W., Fusco, A. C., Brenninkmeijer, C. A. M., Prather, M. J., Wofsy, S. C., and McElroy, M. B.: Three-dimensional climatological distribution of tropospheric OH:

Update and evaluation, J. Geophys. Res., 105, 8931–8980, 2000.
Swoboda, A. R. and Kunze, G. W.: Reactivity of montmorillonite surfaces with weak organic bases, Soil Sci. Soc. Amer. Proc., 32, 806–811, 1968.
Tegen, I. and Fung, I.: Modeling of mineral dust in the atmosphere: sources, transport, and optical thickness, J. Geophys. Res., 99, 22 897–22 914, 1994.
Tie, X., Kao, C.-Y., Miroz, E. J., Cicerone, R. J., Alyea, F. N., and Cunnold, D. M.: Three-dimensional simulations of atmospheric methyl chloroform: effect of an ocean sink, J. Geophys. Res., 97, 20 751–20 769, 1992.
Theng, B. K. G.: The chemistry of clay-organic reactions, Adam hilger, London, 1974.
Underwood, G. M., Song, C. H., Phadnis, M., Carmichael, G. R., and Grassian, V. H.: Heterogeneous reactions of NO_2 and HNO_3 on oxides and mineral dust: A combined laboratory and modeling study, J. Geophys. Res., 106, 18 055–18 066, 2001.
Verrecchia, E. P. and Le Coustumer, M.-N.: Occurrence and genesis of palygorskite and associated clay minerals in a Pleistocene calcrete complex, Sde Boqer, Negev Desert, Israel, Clay Miner., 31, 183–202, 1996.
Vogel, T. M., Criddle, C. S., and McCary, P. L.: Transformation of halogenated aliphatic compounds, Environ. Sci. Technol., 21, 722–736, 1987.
Weissman, M. and Benson, S. W.: HCl elimination from C_2HCl_5: evidence for an abnormally high activation energy caused by beta-chlorine substitutes, Int. J. Chem. Kinet., 16, 941–945, 1984.
WMO: Scientific assessment of ozone depletion: 1988, volume 1, in WMO global ozone research and monitoring project – report no. 44, 1.1–1.54, 1998.
Zielke, R. C., Pinnavaia, T. J., and Mortland, M. M.: Adsorption and reactions of selected organic molecules on clay mineral surfaces, in Reactions and movement of organic chemicals in soils, SSSA Special Publication Number 22, edited by B. L. Sawhney and K. Brown, Soil Science Society of America and American Society of Agronomy, Madison, Wisconsin, 81–97, 1989.

Table 1. Standard clay samples examined. Their multi-plot (Eq. 1) and general (Eq. 2) BET surface area, and the reactivity against heterogeneous decomposition of CH_3CCl_3 in air at 313 K

Locality	API No.	BET plot (Eq. 1) area ($m^2\ g^{-1}$)	BET plot (Eq. 1) C	g-BET plot (Eq. 2) area ($m^2\ g^{-1}$)	g-BET plot (Eq. 2) C	g-BET plot (Eq. 2) n	$10^5\ k_1$ (s^{-1} (50mg)$^{-1}$)	$10^5\ k_1\ /\ s$ ($s^{-1}\ m^{-2}$)	100K	N
blank (no clay)							0.05 (0.10)		−1.0	1
Kaolinite										
Bath, S.C.	5	18.5	145	18.7	79	10	2.72 (0.12)	2.91 (0.13)	4.4	1
Bath, S.C.	7	26.2	170	26.6	86	10	2.73 (0.12)	2.06 (0.09)	1.5	1
Lewistown, Mont.	17	8.7	148	8.7	75	10	0.97 (0.11)	2.23 (0.25)	0.8	1
Halloysite										
Bedford, Ind.	12	55.2	576	56.6	166	4.3	8.17 (0.15)	2.89 (0.05)	9.5	1
Wagon Wheel Gap, Colo.	29	38.3	38	38.3	42	10	3.70 (0.12)	1.93 (0.06)	3.7	1
Dickite										
San Juanito, Mexico	15	1.8	40	1.9	18	10	0.06 (0.10)	0.58 (1.02)	−1.6	1
Montmorillonite										
Forest, Miss.	20	97.1	−487	105.	181	2.5	41.0 ± 14.7	7.78 ± 2.80	20.6	3
Forest, Miss.	21	92.3	−474	100.	183	2.5	29.31 (0.92)	5.86 (0.18)	33.9	1
Amory Miss.	22	78.9	−870	94.0	205	2.9	16.52 (0.58)	3.87 (0.14)	42.8	1
Amory, Miss.	22A	78.9	−342	85.3	296	2.6	17.53 (0.59)	3.73 (0.13)	40.9	1
Chambers, Ariz.	23	69.3	−163	73.6	171	2.9	26.60 (0.81)	7.23 (0.22)	31.8	1
Otay, Calif.	24	32.4	314	33.5	105	4.1	6.48 (0.30)	3.87 (0.18)	10.2	1
Upton, Wyo.	25	18.6	750	19.1	173	4.0	1.04 (0.24)	1.09 (0.25)	1.9	1
Clay Spur, Wyo.	26	25.0	166	25.7	83	10	1.03 (0.24)	0.80 (0.19)	1.0	1
Belle Fourche, S. Dak.	27	21.2	−1310	22.1	251	3.3	1.67 ± 0.28	1.51 ± 0.25	2.3	2
Santa Rita, N. Mex.	30	33.7	−2438	35.7	180	3.2	3.40 (0.31)	1.91 (0.17)	18.7	1
Bayard, N. Mex.	30A	65.8	−408	71.4	231	2.6	12.40 (0.49)	3.47 (0.14)	36.3	1
Cameron, Ariz.	31	30.5	−484	32.9	200	2.6	7.42 (0.32)	4.51 (0.19)	10.6	1
Metabentonite										
Tazewell, Va.	41	16.5	1847	17.4	126	3.1	5.15 (0.28)	5.92 (0.33)	9.1	1
Nontronite										
Garfield, Wash.	33A	36.5	−529	38.8	269	2.8	16.23 (0.41)	8.37 (0.21)	20.5	1
Manito, Wash.	33B	58.1	−506	66.3	239	2.7	20.92 (0.51)	6.31 (0.15)	27.9	1
Hectorite										
Hector, Calif.	34	39.5	−241	43.5	277	2.3	48.1 ± 22.3	22.1 ± 10.3	0.76	3
Illite										
Fithian, Ill.	35	61.0	202	63.1	114	3.5	18.6 ± 3.7	5.9 ± 1.2	17.7	2
Fithian, Ill.	35*	69.6	145	70.6	121	4.1	25.8 ± 9.3	7.3 ± 2.6	26.0	5
Morris, Ill.	36	44.8	218	45.7	100	10	2.9 ± 0.3	1.3 ± 0.1	6.4	2
Pyrophyllite										
Robbins, N. C.	49	1.4	27	1.6	12	10	−0.25 (0.17)	−3.1 (2.1)	−1.8	1
results in the previous work										
Kaolinite-p		16.0	44	16.9	23	10	0.26 (0.10)	0.31 (0.12)	0.7	
Halloysite-p		29.4	201	29.9	99	10	3.45 (0.12)	2.31 (0.08)	10.0	
Montmorillonite-p		18.0	51	18.9	27	10	0.56 (0.10)	0.59 (0.10)	1.4	
Allophane-p		234.7	1397	245.8	179	3.3	34.3 (0.8)	2.79 (0.06)	10.8	

Table 2. The values of k_1 and K_H^{MC} measured, and the k_{sr} values calculated for reactions of CH_3CCl_3 in air on illite (API no. 35*) at 283–313 K. The data for all the experimental runs and the mean of them at each temperature were listed

T(K)	k_1 (10^{-5} s^{-1})	K_H^{MC} (10^{16} m^{-2} Pa^{-1})	k_{sr}(10^{-4} s^{-1})
313	11.6	1.13	7.1
	24.0	0.82	19.5
	25.9	0.90	19.6
	35.8	0.52	44.9
	31.9	0.69	30.4
mean	25.8 ±9.3	0.81 ± 0.23	24.3 ± 14.2
298	3.9	2.37	1.4
	11.7	1.61	5.4
	9.2	1.65	4.2
mean	8.3 ± 4.0	1.88 ± 0.43	3.7 ± 2.1
283	1.2	4.21	0.3
	8.5	3.93	2.1
	6.5	3.75	1.7
mean	5.4 ± 3.8	3.97 ± 0.23	1.4 ± 1.0

ACPD

3, 1843–1891, 2003

Table 3. Estimated local lifetime (τ_{dust}^{local}) through the reaction on airborne dust. Blanks mean > 1000 years

T (K)	τ_{dust}^{local} (year)					
$10^6\, n_m$ (g m^{-3})	1	10	50	100	200	500
273				600	300	100
283			600	300	200	60
298			300	100	70	30
313		600	100	60	30	10
328		300	60	30	20	6

ACPD

3, 1843–1891, 2003

Table 4. Estimated tropospheric lifetime (τ_{ground}^{tropos}) through the decomposition on the ground surface. Blanks mean > 1000 years

T (K)	τ_{ground}^{tropos} (year)									
	d_L (μm)	2000			20			2		
	N_d	5	2	0.5	5	2	0.5	5	2	0.5
case (i) C_W = 0.4% by weight										
283		5	10	50	400	1000				
298		3	8	30	200	400				
313		3	6	30	80	200	800	800		
328		2	6	20	40	100	400	400	100	
case (ii) C_W = 100 ppmw										
283		200	400							
298		70	200	700						
313		30	80	300						
328		20	40	200						
case (iii) C_W = 0.4% by weight. In Eq. (20), the value of 0.05 K_A^{MC} is used instead of that of K_A^{MC} calculated by Eq.(17).										
283		80	200	800						
298		40	90	400						
313		20	40	200						
328		9	20	90	800					

ACPD
3, 1843–1891, 2003

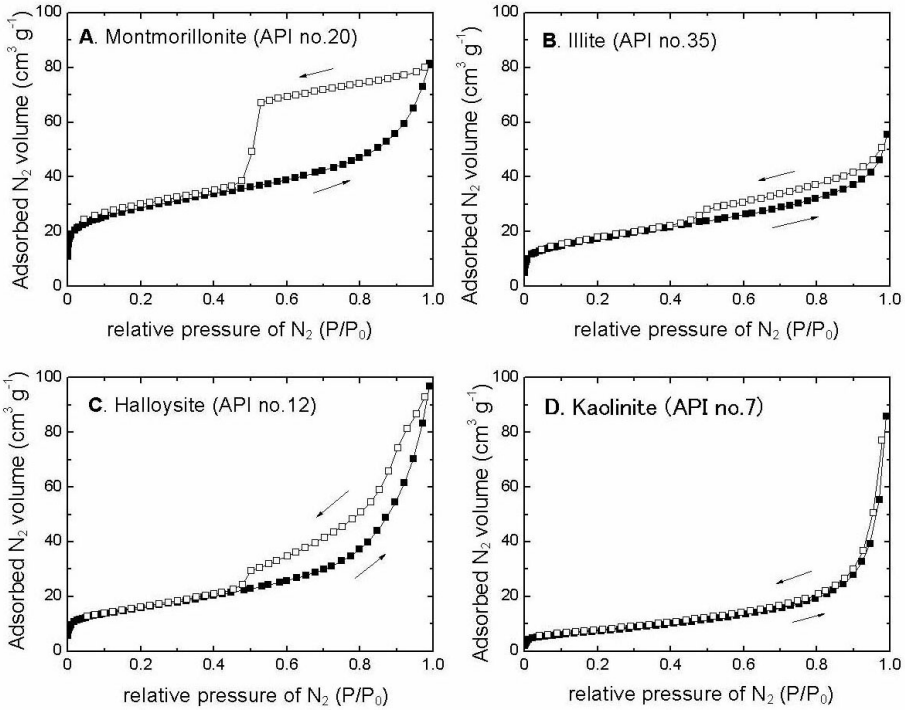

Fig. 1. Nitrogen isotherms for four types of standard clay minerals; solid square, adsorption isotherm; open square, desorption isotherm.

ACPD
3, 1843–1891, 2003

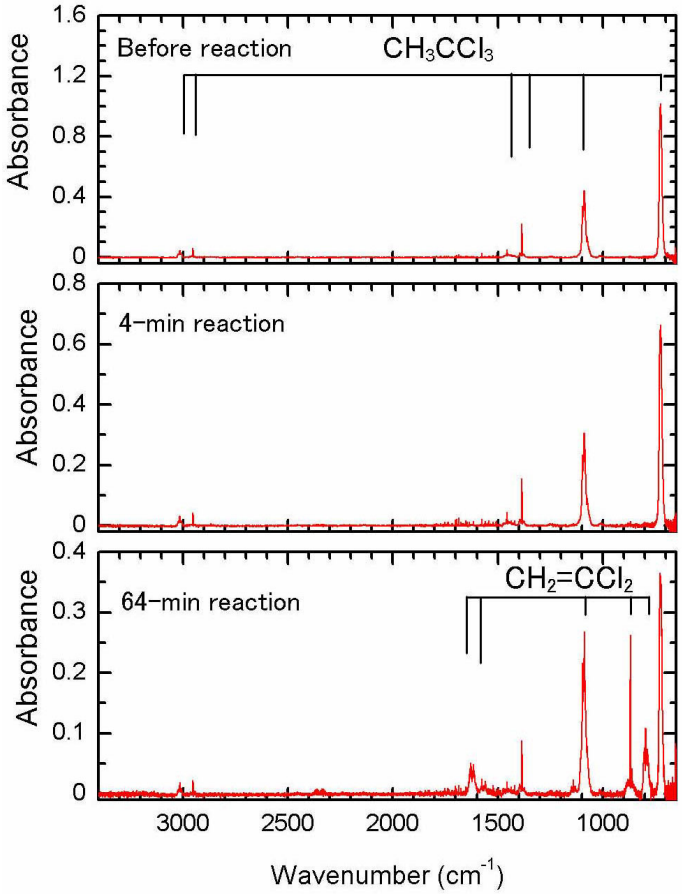

Fig. 2. IR spectra of CH_3CCl_3 and its decomposition products in the gas phase for the reaction of CH_3CCl_3 in air on halloysite (API no. 12) particles at 313 K. **(a)** Before contact with the halloysite, **(b)** after a 4-min, and **(c)** after a 64-min reaction.

ACPD
3, 1843–1891, 2003

Laboratory study on heterogeneous decomposition of methyl chloroform

S. Kutsuna et al.

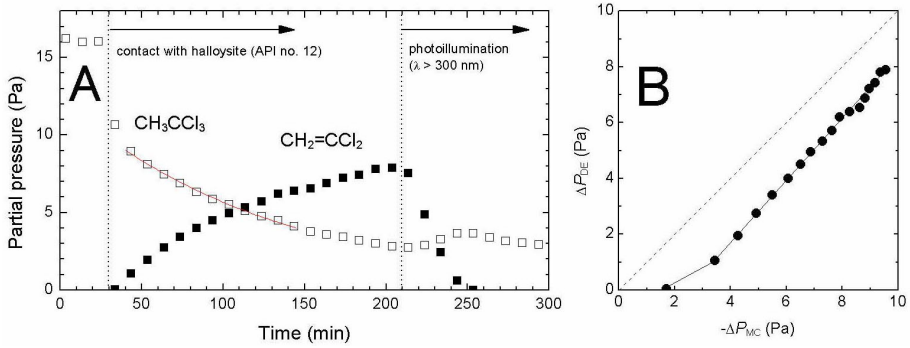

Fig. 3. Changes in CH_3CCl_3 and newly formed $CH_2{=}CCl_2$ for the reaction shown in Fig. 2. **(A)** Time course of CH_3CCl_3 (open symbol) and newly formed $CH_2{=}CCl_2$ (solid symbol) partial pressures. Solid red line is a fit by first-order kinetics. **(B)** The decrease in CH_3CCl_3 partial pressure ($-\Delta P_{MC}$) versus the increase in $CH_2{=}CCl_2$ partial pressure (ΔP_{DE}) during a 180-min reaction without photoillumination.

ACPD
3, 1843–1891, 2003

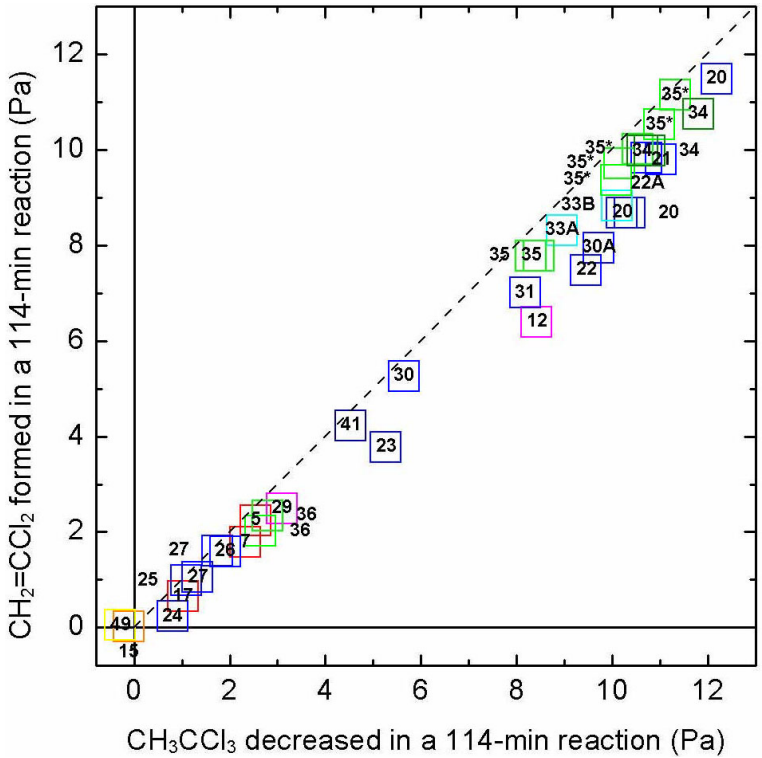

Fig. 4. The decrease in CH_3CCl_3 partial pressure ($-\Delta P_{MC}$) versus the increase in $CH_2{=}CCl_2$ partial pressure (ΔP_{DE}) for 114-min reactions on various API standard clay minerals at 313 K. The label indicates the API number of the clay minerals. Clay minerals of the same type are represented by the same color.

ACPD

3, 1843–1891, 2003

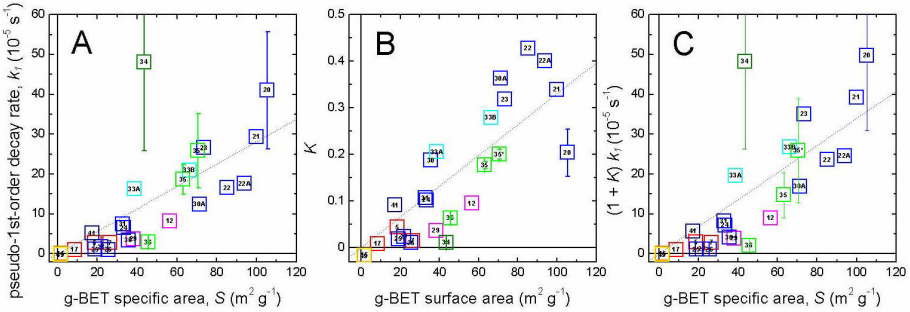

Fig. 5. (A) Pseudo-first-order rate constant k_1, **(B)** removal ratio due to the adsorption K, and **(C)** $(1+K)\,k_1$ in reactions on various API standard clay minerals at 313 K versus specific surface area S of each clay mineral deduced by Eq. (2). The label indicates the API number of the clay minerals. Clay minerals of the same type are represented by the same color.

ACPD
3, 1843–1891, 2003

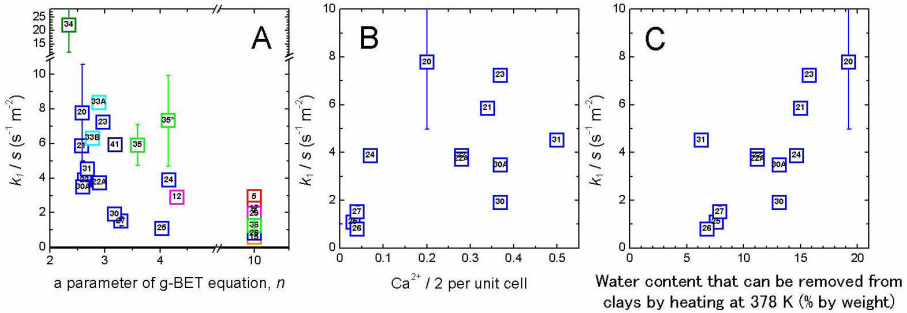

Fig. 6. (A) The k_1/s value in reactions on various API standard clay minerals at 313 K versus a parameter of the general BET equation, n. **(B)** The k_1/s value versus interlayer Ca^{2+} in a unit cell of the clay minerals (Kerr et al., 1950). **(C)** The k_1/s value versus amount of H_2O released from clay minerals by heating at 378 K in per cent by weight (Kerr et al., 1950).

ACPD
3, 1843–1891, 2003

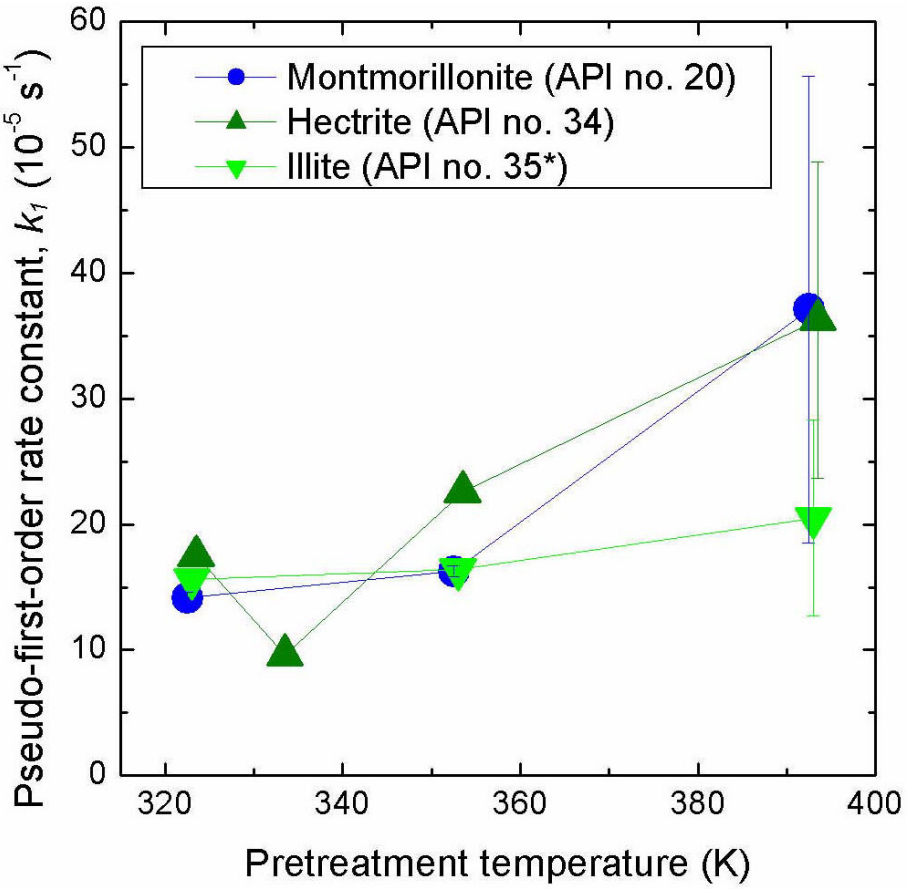

Fig. 7. The pseudo-first-order reaction rate in reactions on clay minerals at 313 K versus the pretreatment temperature of clay minerals. The pretreatment temperature means the temperature at which montmorillonite (API no. 20), hectorite (API no. 34), or illite (API no. 35*) was heated before the reaction.

ACPD
3, 1843–1891, 2003

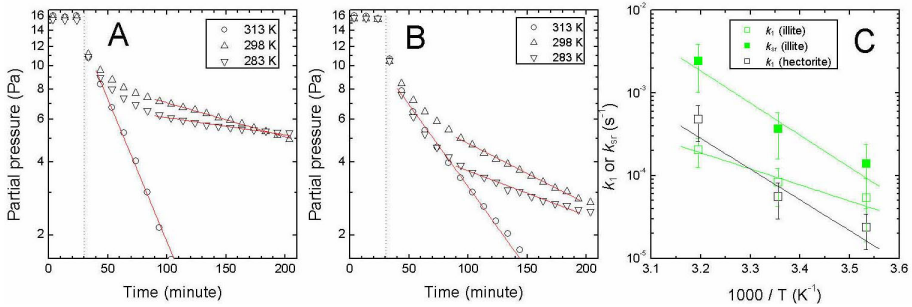

Fig. 8. (A) Semi-log plot of the time course of CH_3CCl_3 partial pressures for the reactions on hectorite (API no. 34) and **(B)** on illite (API no. 35*) at 283–313 K. **(C)** The k_1 values averaged for the reaction on hectorite (API no. 34) and the k_1 and k_{sr} values averaged for the reaction on illite (API no. 35*) versus the inverse of reaction temperatures; open square, k_1; solid square, k_{sr}.

ACPD
3, 1843–1891, 2003

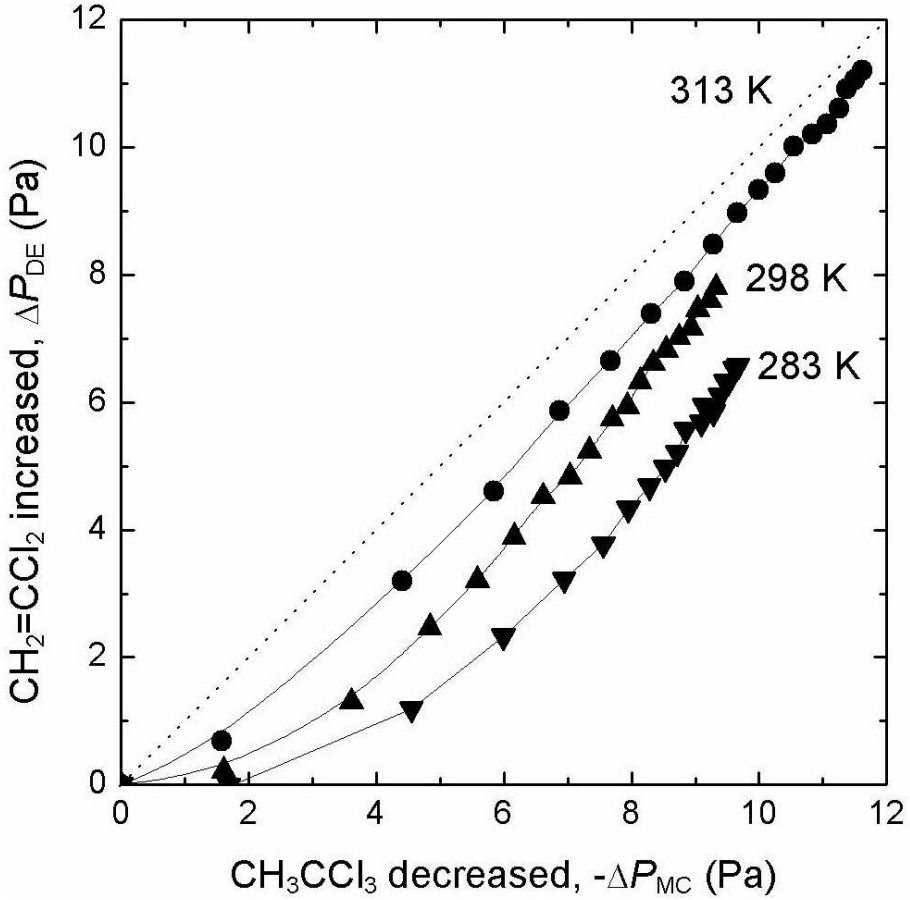

Fig. 9. The decrease in CH_3CCl_3 partial pressure ($-\Delta P_{MC}$) versus the increase in $CH_2=CCl_2$ partial pressure (ΔP_{DE}) during reactions on illite (API no. 35*) materials at 283, 298, and 313 K.

ACPD

3, 1843–1891, 2003

Laboratory study on heterogeneous decomposition of methyl chloroform

S. Kutsuna et al.

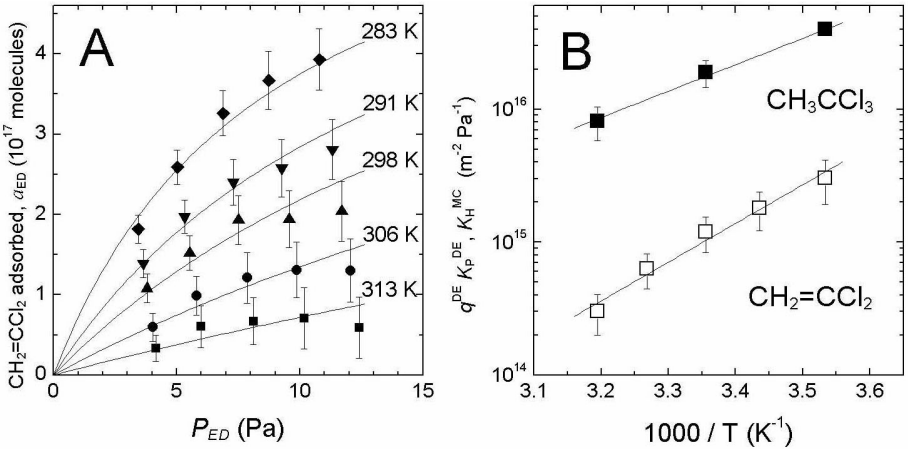

Fig. 10. Adsorption on illite (API no. 35*). **(A)** Isotherms of CH_2=CCl_2 in air at 283–313 K. **(B)** The temperature dependence of the adsorption parameters for CH_2=CCl_2 (open symbols) and CH_3CCl_3 (solid symbols).

ACPD
3, 1843–1891, 2003

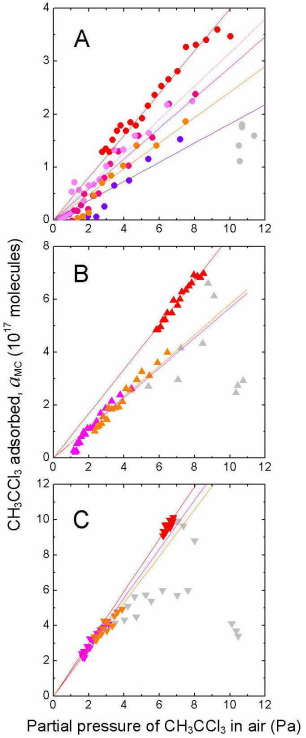

Fig. 11. The amount of CH_3CCl_3 adsorbed on illite (API no. 35*) versus the partial pressure of CH_3CCl_3 in the reactions of CH_3CCl_3-air mixtures on illite (API no. 35*) materials at **(A)** 313 K, **(B)** 298 K, and **(C)** 283 K. Different colors in each part of the figure indicate the data for different experimental runs. Solid lines are fits by Eq. (8) in the text. Gray symbols are data used during the initial reaction periods, but they were not fitted.

ACPD
3, 1843–1891, 2003

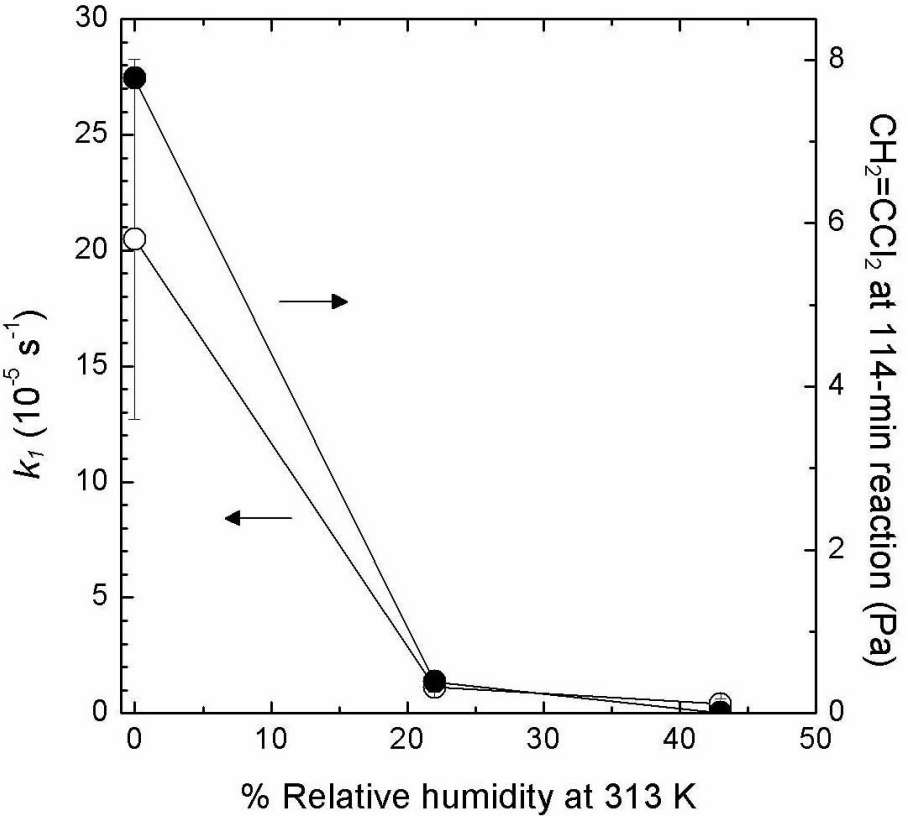

Fig. 12. The effects of the relative humidity on a reaction of a CH_3CCl_3-air mixture on illite (API no. 35*) materials at 313 K. Open symbols represent the pseudo-first-order rate constant; solid symbols represent the amount of $CH_2=CCl_2$ produced in a 114-min reaction.

ACPD

3, 1843–1891, 2003

Laboratory study on heterogeneous decomposition of methyl chloroform

S. Kutsuna et al.

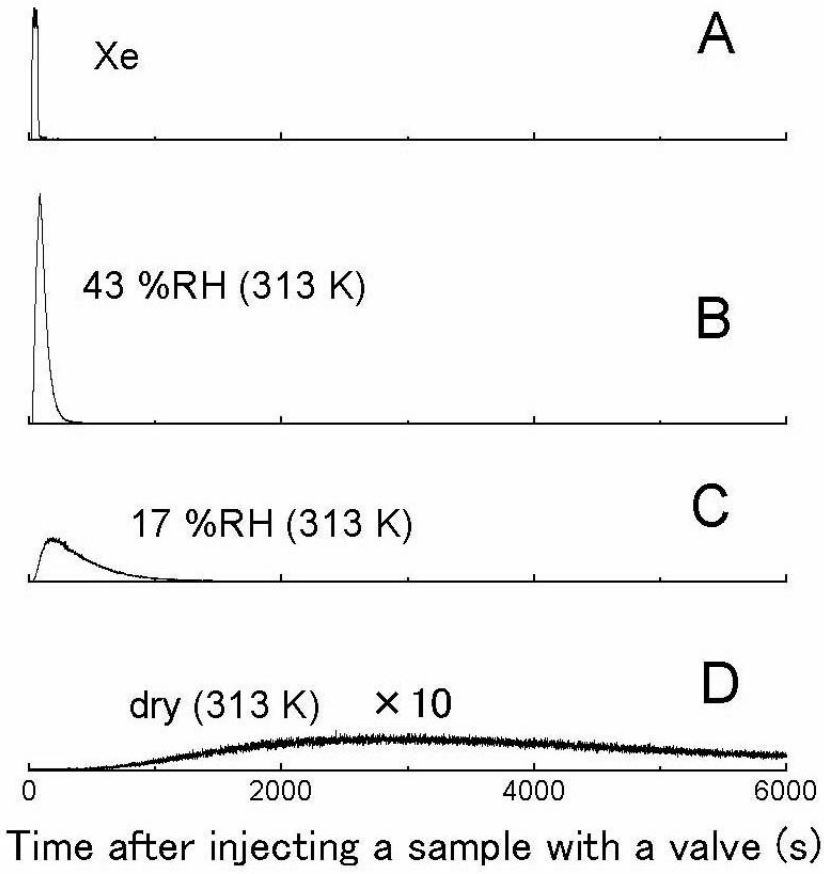

Fig. 13. The results of the column experiment for illite (no. 35*) in dry or humidified He flow at 313 K. **(A)** The experiment of a Xe-He mixture in dry He flow. **(B)–(D)** The experiments of a CH_3CCl_3He mixture in (B) 43% RH, (C) 17% RH, and (D) dry He flow.

ACPD
3, 1843–1891, 2003